Article

Classification of Variable Star Light Curves with Convolutional Neural Network

Almat Akhmetali [ID], Timur Namazbayev [ID], Gulnur Subebekova *[ID], Marat Zaidyn, Aigerim Akniyazova [ID], Yeskendyr Ashimov [ID] and Nurzhan Ussipov [ID]

Department of Electronics and Astrophysics, Al-Farabi Kazakh National University, 050040 Almaty, Kazakhstan; akhmetalialmat@gmail.com (A.A.); timur.namazbayev@gmail.com (T.N.); zaidyn_marat@kaznu.edu.kz (M.Z.); aigerimakniyazova@gmail.com (A.A.); ashimov.yeskendyr@kaznu.kz (Y.A.); ussipov.nurzhan@kaznu.kz (N.U.)
* Correspondence: gulnursubebekova@gmail.com

Abstract: The classification of variable stars is essential for understanding stellar evolution and dynamics. With the growing volume of light curve data from extensive surveys, there is a need for automated and accurate classification methods. Traditional methods often rely on manual feature extraction and selection, which can be time-consuming and less adaptable to large datasets. In this work, we present an approach using a convolutional neural network (CNN) to classify variable stars using only raw light curve data and their known periods, without the need for manual feature extraction or hand-selected data preprocessing. Our method utilizes phase-folding to organize the light curves and directly learns the variability patterns crucial for classification. Trained and tested on the Optical Gravitational Lensing Experiment (OGLE) dataset, our model demonstrates an average accuracy of 88% and an F1 score of 0.89 across five well-known classes of variable stars. We also compared our classification model with the Random Forest (RF) classifier and showed that our model gives better results across all of the classification metrics. By leveraging CNN, our approach does not need manual feature extraction and can handle diverse light curve shapes and sampling cadences. This automated, data-driven method offers a powerful tool for classifying variable stars, enabling efficient processing of large datasets from current and future sky surveys.

Keywords: variable star; light curve; machine learning; convolutional neural network; random forest

1. Introduction

Variable stars play a crucial role in expanding our understanding of the universe, contributing to various fields including stellar astrophysics, galactic astrophysics, and cosmology. They have been instrumental in key discoveries, such as determining distances to galaxies, measuring the Hubble constant, studying stellar evolution, investigating planetary formation, and studying the chemical composition of different galactic regions [1–11]. To study these stars effectively, modern astronomical surveys have provided massive datasets. With the advent of advanced astronomical instrumentation and large-scale time-domain surveys like the Optical Gravitational Lensing Experiment (OGLE) [12–15], the All-Sky Automated Survey (ASAS) [16], the Catalina Real-Time Transient Survey (CRTS) [17,18], the Zwicky Transient Facility (ZTF) [19,20], and NASA's Kepler mission [21], the volume of time-series data available has surged dramatically. These datasets, consisting of light curves that capture the brightness of stars over time, are invaluable for studying variable stars. However, the sheer quantity and complexity of these data necessitate automated classification methods. The automatic classification of variable stars allows astronomers to maximize the scientific return from these surveys, especially as manual classification is impractical given the sheer volume of data.

Traditional approaches to classifying variable stars often rely on extracting features from the light curves, such as statistical descriptors, period analysis, and Fourier decomposition parameters [22]. These features condense the information of each light curve into

into feature sets for machine learning (ML) classification. While effective, feature extraction methods can be computationally expensive and are often tailored to specific survey data, limiting their adaptability. Furthermore, these approaches may struggle with light curves that are sparse, noisy, or unevenly sampled due to observational constraints, making the classification process more complex and less reliable across different datasets.

In recent years, there has been a significant increase in the development of automated methods for classifying variable star light curves. A prevalent strategy for automated classification involves extracting periodic and non-periodic features from light curves and inputting them into ML classifiers. Periodic features typically include period and Fourier decomposition parameters, while non-periodic features are often statistical parameters.

For instance, an automated method by Debosscher et al. [23] utilized 28 features derived from the Fourier analysis of time-series data, focusing primarily on amplitudes, phases, and frequencies obtained from the Fourier fit, which were then fed into Gaussian Mixture and ML classifiers for supervised learning. Similarly, Kim et al. [24] focused on detecting Quasi-Stellar Objects (QSOs) within the MACHO [25] dataset. They found that the Random Forest (RF) [26] classifier outperformed the Support Vector Machine (SVM) [27] using 11 features. In the same year, Richards et al. [28] reached similar conclusions after evaluating 53 features by combining the periodic features with the non-periodic features proposed by Butler and Bloom [29]. They demonstrate the use of various ML-based classifiers for the automatic classification of a large number of variability classes. Additionally, they explored hierarchical classification methods, employing hierarchical single-label classification (HSC) and hierarchical multi-label classification (HMC) with RFs. Kim and Bailer-Jones developed a package called UPSILoN, which extracts 16 features from light curves and classifies them using the RF technique [30]. More recent studies continue to employ these techniques to identify specific classes of variability [31,32].

Feature-based classification methods have demonstrated high accuracy but inherently assume that a sufficient number of timestamps are available for a given light curve. For instance, UPSILoN suggests that a light curve should have over 80 data points to achieve satisfactory precision and recall. However, many light curves from astronomical surveys are noisy and contain temporal gaps due to observational constraints and survey design. Additionally, differences in cadence among various surveys can make the feature extraction and classification processes heterogeneous and survey-dependent.

Instead of using hand-crafted features, recent studies have shifted focus towards leveraging raw time-series data within advanced deep learning (DL) frameworks. For example, Mahabal et al. [33] processed raw light curves to generate $dm - dt$ maps, which captured the differences between magnitudes (dm) and corresponding time-stamps (dt) for each pair in the light curve. These differences were binned into fixed dm and dt ranges to create uniform attributes for each light curve, which were then mapped into a two-dimensional image and fed into a CNN for training.

Naul et al. [34] utilized a recurrent neural network (RNN)-based autoencoder for unsupervised feature extraction, effectively capturing essential information from light curves. They leveraged latent features from the encoding layers as a compressed representation with reduced dimensionality, addressing the challenge of variable light curve lengths that many ML/DL classifiers face. They observed that working with period-folded light curves enhances the accuracy of the encoding–decoding process, allowing for more refined feature extraction. Consequently, they employ latent features from the folded light curves for further classification through an Rf model.

Aguirre et al. [35] proposed generating two vectors: one for time differences and another for magnitude differences, derived from each light curve. These vectors were combined into a matrix, which was input into a 1D CNN for training. In this setup, the time and magnitude vectors act as individual channels, similar to the way color channels function in image data. Carrasco-Davis et al. [36] applied a recurrent convolutional neural network (RCNN) to image sequences, achieving a recall of 94 percent on data from the

High Cadence Transient Survey (HiTS). Likewise, Becker et al. [37] implemented RNNs to classify the main types of variability, reaching an accuracy of 95%.

To address the challenge of static classification models, which require re-training as new data become available, Zorich et al. [38] introduced a probabilistic classification model for light curves that accommodates a continuous stream of data. They applied this approach to data from the CoRot, OGLE, and MACHO catalogs.

In this work, we propose a neural network that can leverage the vast amount of data available from surveys, while reducing the preprocessing needed to perform an automatic classification of variable stars. Our approach does not require feature computation, can scale to vast amounts of data, and only needs the known periods alongside the light curves. We present our experimental analysis using the OGLE dataset.

The rest of the paper is organized as follows. In Section 2, we describe the data used in this work for training and testing, the classification models, and the preprocessing steps required for CNN implementation. Section 3 provides information about the structure of the used neural network. In Section 4, we present and discuss results. Section 5 concludes the article.

2. Dataset and Preprocessing

2.1. Optical Gravitational Lensing Experiment (OGLE)

We obtained the time-series data from the OGLE survey, which is one of the most comprehensive datasets available [12–15]. It operated in its third phase from 2001 to 2009. This phase focused on the Galactic bulge, disk, and Magellanic Clouds, classifying over 450,000 variable stars. Observations were conducted in the *V* and *I* bands, with the *I* band having ten times more observations than the *V* band; therefore, we only used the *I* band. This catalog is considered highly reliable, as all objects were confirmed by experts, and the light curves are well defined with high signal-to-noise ratios in most observations.

We only selected a few of classes which have an adequate number of distinct light curves (∼500 or more) for the stable training of the classification model. Rather than attempting to compile all known variable star classes, as attempted with limited success by [23], we focused our research on a subset of five well-studied classes. The five chosen classes are Classical Cepheids, *δ* Scuti, Mira, RR Lyrae and Eclipsing Binaries. Typical phase-folded light curves for each class are presented in Figure 1.
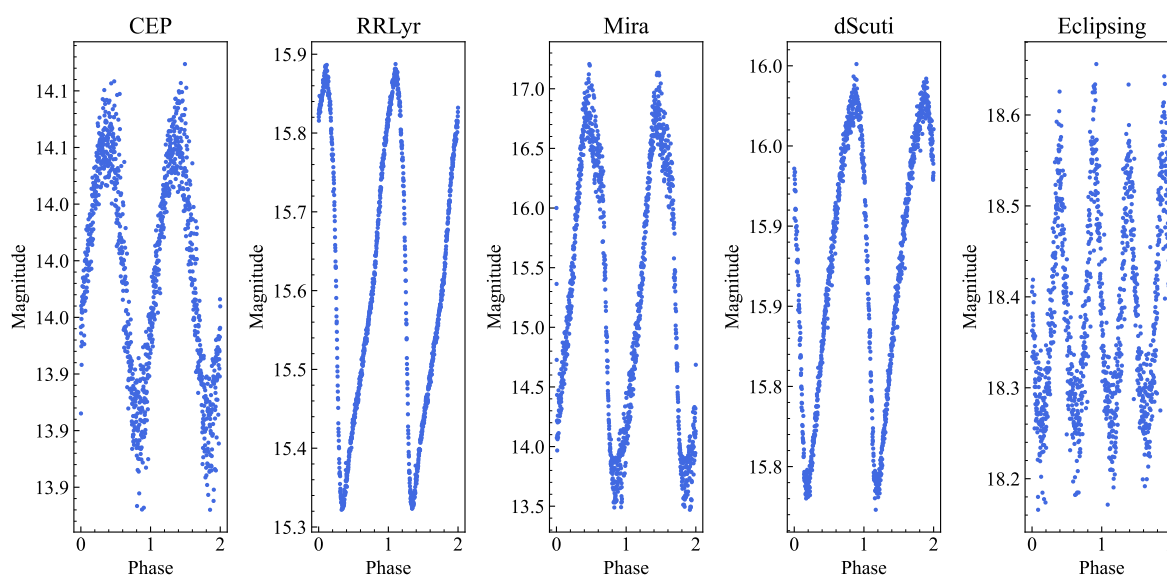

Figure 1. Example of variable stars in the Classical Cepheids, *δ* Scuti, Mira, RR Lyrae and Eclipsing Binaries selected in the training and testing set.

To ensure that our network has enough data points to uncover correlations and extract meaningful features for variability classification, we limited our selection to light curves with at least 500 data points. From the OGLE database, which includes 165,105 light curves for Eclipsing Binaries, we only chose 50,000 to prevent their overwhelming influence in training and to keep computation manageable (although this class still had a larger representation than the other four classes). Our final dataset from OGLE comprised a total of 122,229 light curves. A breakdown of the selected light curves for each variability class is shown in Table 1, with Figure 2 providing a visual representation to better illustrate the dataset. Additionally, we removed single-point outliers that deviated by more than 3σ, as these were likely due to instrumental effects.

Table 1. Total numbers of light curves per class in our dataset.

Class	Representation	Number
Classical Cepheids	CEP	4776
δ Scuti	dScuti	20,000
Mira	Mira	15,701
RR Lyrae	RR Lyr	31,752
Eclipsing	Eclipsing	50,000
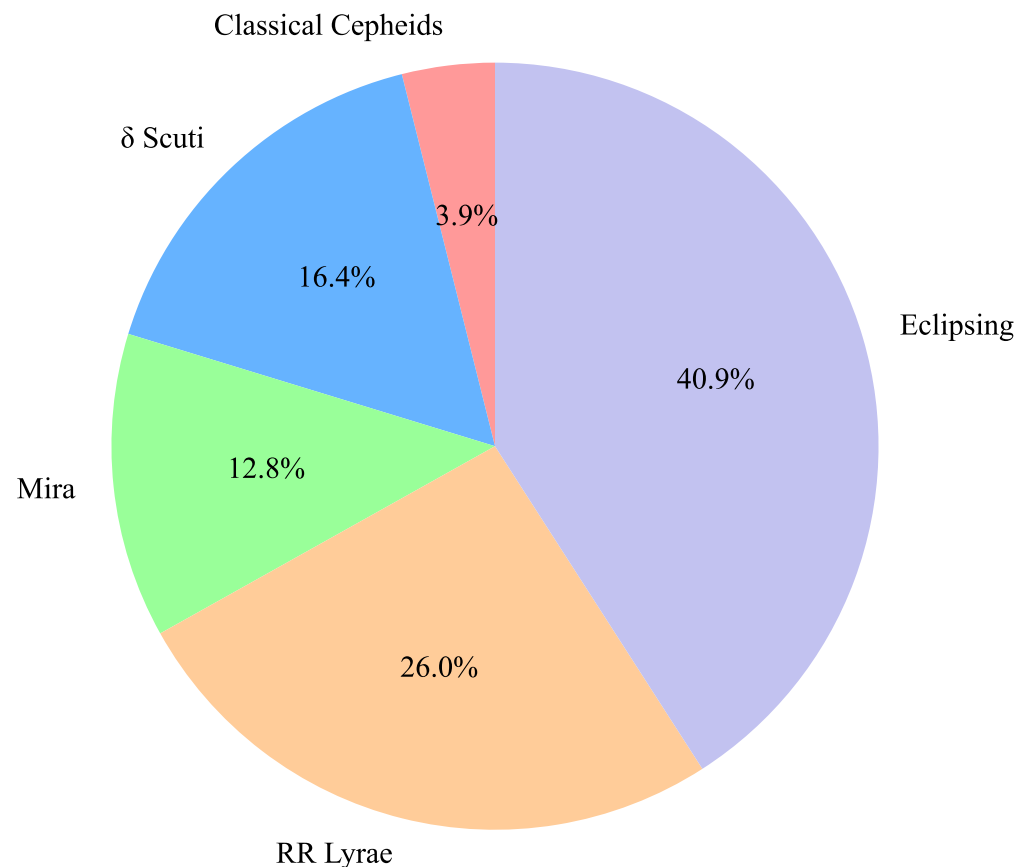
Figure 2. Distribution of light curves per class in the dataset. Eclipsing variables dominate with 40.9% of the total light curves, followed by RR Lyrae (26%), δ Scuti (16.1%), Mira (12.6%), and Classical Cepheids (3.9%).

2.2. Padded Phase-Folded Light Curves

The primary reason for choosing a 1D CNN model is that light curves are represented as one-dimensional sequences, and altering or reordering them can risk losing valuable information. For periodic variability, as we observe in our dataset where periods are known, using a phase-folded light curve offers greater insights than the raw data. This is illustrated

in Figure 3, showing a Classical Cepheid light curve from the OGLE survey. While the left panel displays the raw light curve without a clear pattern, the right panel presents a distinct sinusoidal pattern, highlighting the periodic nature. Consequently, the phase-folded light curve is more informative and enhances the model's ability to learn meaningful patterns.

We propose a 1D CNN model that utilizes phase-folded light curves as input. However, this classification model requires all input sequences to have uniform lengths. To achieve this, we employed a strategy of zero-padding at the end of the light curves to standardize their lengths. If the length of a light curve exceeded a predefined threshold, it was truncated accordingly. Conversely, for light curves shorter than the threshold, zero-padding was applied to extend them to the required length. This preprocessing step ensures consistency across all phase-folded light curve inputs for the model. The next consideration was determining the appropriate threshold length for the light curves. This length must be sufficient to preserve the critical information within the light curves, ensuring that they remain informative for classification. Simultaneously, it should not be excessively long, as this would increase computational complexity and processing time. Finding the right balance between preserving information and optimizing computational efficiency is essential for the model's performance.

Light Curve ID: OGLE-SMC-CEP-4998
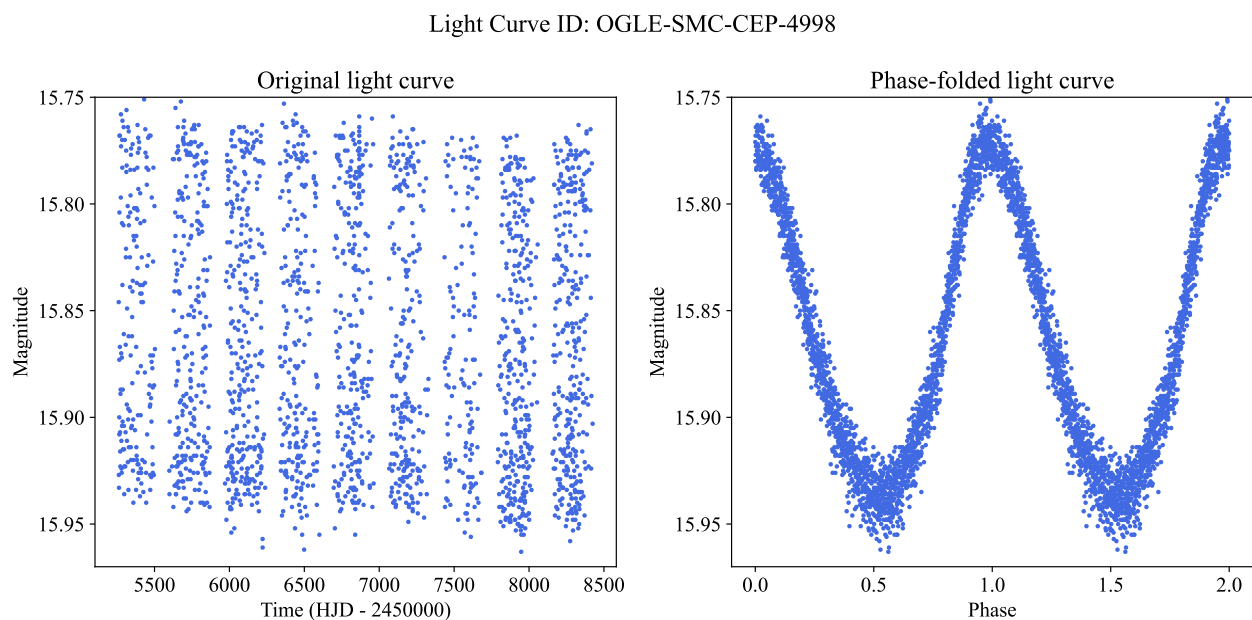
Figure 3. Light curve for a Classical Cepheid from the OGLE survey. The left panel shows the original light curve whereas the right panel shows the phase-folded light curve with an estimated period of 0.34 days. The light curve ID is mentioned as the title of the plot.

To determine the appropriate threshold length, we examined the distribution of the light curve lengths in our dataset, as shown in Figure 4. The most frequent length, representing the typical number of observations per object, is 1150. We recognize that this length is sufficient for the model to learn meaningful patterns while being short enough to avoid excessive computational overhead.

Figure 4. Distribution of light curve lengths (number of observations) in the dataset. The inset highlights the most common range of observations, with the peak occurring around 1150 observations.
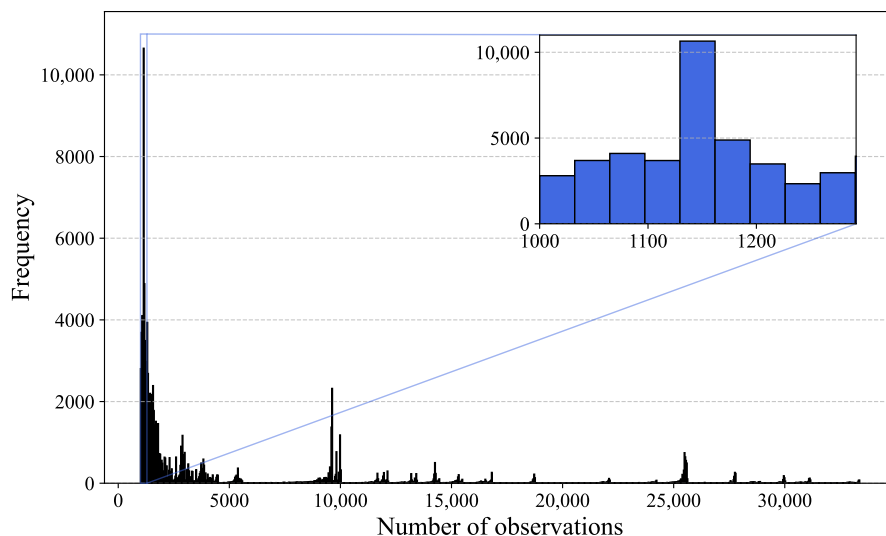
3. Convolutional Neural Network

Convolutional neural networks (CNNs or ConvNets) [39–41] are widely recognized as powerful tools for pattern recognition in various astronomical data domains [42–44]. They have been extensively employed in astronomy for both classification and regression tasks. Numerous studies have demonstrated that deep learning frameworks, such as CNNs, often outperform traditional ML algorithms [45,46].

A CNN is a type of deep neural network specifically designed for feature extraction and pattern recognition in image data. It comprises an input layer, an output layer, and several hidden layers, including convolutional, activation, pooling, fully connected, and normalization layers. Convolutional layers apply filters to input data, generating feature maps that are passed to subsequent layers. Pooling layers, such as MaxPooling, reduce the dimensionality of feature maps by selecting the maximum value in a region, thereby, aiding in generalization and accelerating the training process. Alternatively, Average Pooling uses the average value within the pooling window. Fully connected layers interpret the extracted features from previous layers, with each neuron connected to every activation from the preceding layer. Normalization layers help to stabilize learning by adjusting activations, which also prevents overfitting.

In this work, we utilized the CNN architecture described in [47], as illustrated schematically in Figure 5. Our CNN model consists of seven convolutional blocks followed by two dense layers, with a softmax activation function applied at the output layer. Each convolutional block includes a 1D convolution layer with ReLU activation and a 1D MaxPooling layer. The Conv1D layer uses a kernel size of 3, while the MaxPooling1D layer has a pool size of 2, and both layers use the same padding. The convolutional layers are configured sequentially with filter sizes of 128, 64, 32, 32, 32, 32, and 32. The dense layers comprise 64 neurons in the hidden layer and 5 neurons in the output layer, activated by Softmax. This model has a total of 60,517 parameters. We implemented and trained the CNN using TensorFlow 2.1 [48] (Google Brain, Mountain View, CA, USA), optimizing it with the Adam optimizer [49] at a learning rate of 0.001 and a batch size of 32. Categorical cross-entropy was chosen as the loss function. Training was conducted for 100 epochs, with each epoch taking approximately 8 s.
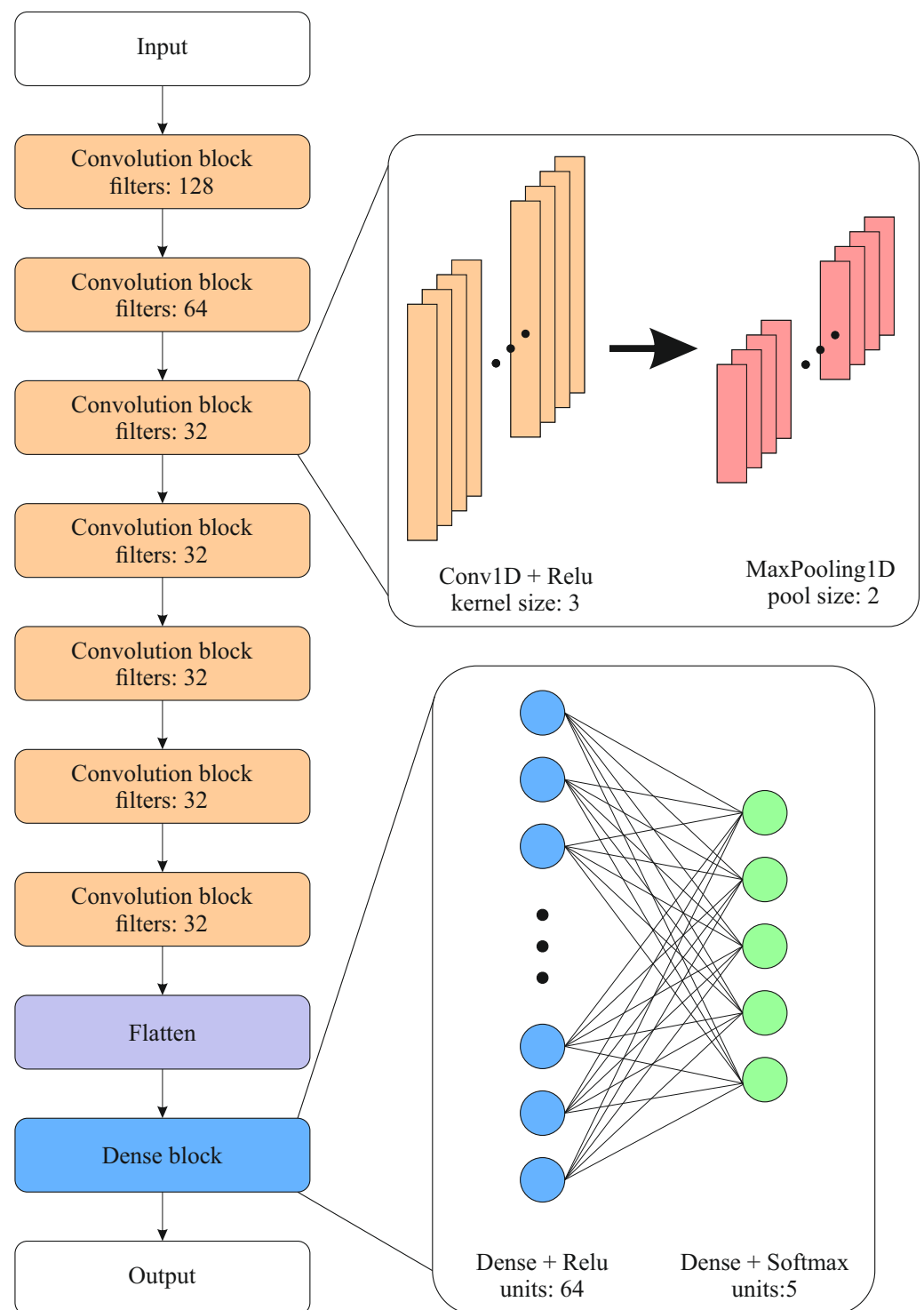
Figure 5. Schematic diagram showing the architecture of CNN.

4. Results and Discussion

Our experiments aimed to evaluate the classification accuracy. We tested our model and compared it with RF. For these models, we present the results obtained by using 80% of the labeled set as a training set and the remaining 20% as a testing set, preserving the percentage of samples for each class in the original labeled set. For training the classification model described in Section 3 and RF, we use a single NVIDIA GeForce RTX 4070 Ti GPU with 12 GB of video memory. The RF classifier wass implemented with default parameters via the Scikit − learn library [50].

Tables [2](#) and [3](#) list four different scores: accuracy, precision, recall, and F1 score. For an individual class, these scores are defined as:

$$\text{Accuracy}_i = \frac{\text{TP}_i + \text{TN}_i}{\text{TP}_i + \text{TN}_i + \text{FP}_i + \text{FN}_i} \tag{1}$$

$$\text{Precision}_i = \frac{\text{TP}_i}{\text{TP}_i + \text{FP}_i}, \tag{2}$$

$$\text{Recall}_i = \frac{\text{TP}_i}{\text{TP}_i + \text{FN}_i}, \tag{3}$$

$$\text{F1 score}_i = 2 \times \frac{\text{Precision}_i \times \text{Recall}_i}{\text{Precision}_i + \text{Recall}_i}, \tag{4}$$

where TP_i denotes the count of true positives, FP_i represents the count of false positives, and FN_i indicates the count of false negatives for a specific class i. Although the labeled dataset exhibits significant imbalance, each class is considered equally important; therefore, we calculated averaged scores:

$$\text{Accuracy}_{\text{average}} = \frac{1}{n_{cl}} \sum_{i=1}^{n_{cl}} \text{Accuracy}_i, \tag{5}$$

$$\text{Precision}_{\text{average}} = \frac{1}{n_{cl}} \sum_{i=1}^{n_{cl}} \text{Precision}_i, \tag{6}$$

$$\text{Recall}_{\text{average}} = \frac{1}{n_{cl}} \sum_{i=1}^{n_{cl}} \text{Recall}_i, \tag{7}$$

$$\text{F1 score}_{\text{average}} = \frac{1}{n_{cl}} \sum_{i=1}^{n_{cl}} \text{F1 score}_i. \tag{8}$$

where n_{cl} represents the total number of classes.

Table 2. Classification metrics (mean $\pm$ standard deviation) of our CNN model. The values and errors were obtained from 5 runs using the k-fold cross-validation method.

Class	Accuracy, %	Precision	Recall	F1 Score
CEP	81.59 ± 0.64	0.84 ± 0.01	0.82 ± 0.01	0.83 ± 0.01
RR Lyr	85.11 ± 0.89	0.87 ± 0.01	0.85 ± 0.01	0.86 ± 0.01
Mira	98.05 ± 0.38	0.99 ± 0.01	0.98 ± 0.01	0.98 ± 0.01
dScuti	80.75 ± 1.84	0.87 ± 0.02	0.81 ± 0.02	0.84 ± 0.01
Eclipsing	94.28 ± 0.39	0.89 ± 0.01	0.94 ± 0.00	0.92 ± 0.01
Average	87.96	0.89	0.88	0.89

Table 3. Classification metrics (mean $\pm$ standard deviation) of RF. The values and errors were obtained from 5 runs using the k-fold cross-validation method.

Class	Accuracy, %	Precision	Recall	F1 Score
CEP	70.56 ± 1.56	0.74 ± 0.02	0.71 ± 0.02	0.72 ± 0.01
RR Lyr	75.67 ± 0.29	0.77 ± 0.01	0.76 ± 0.01	0.76 ± 0.01
Mira	94.11 ± 0.43	0.98 ± 0.01	0.94 ± 0.01	0.96 ± 0.01
dScuti	58.20 ± 0.65	0.92 ± 0.01	0.58 ± 0.01	0.71 ± 0.01
Eclipsing	90.92 ± 0.19	0.77 ± 0.01	0.91 ± 0.01	0.84 ± 0.01
Average	78.69	0.84	0.78	0.80

For the case of our classifier, the averaged accuracy, precision, recall, and F1 score have a value of 0.88, 0.88, 0.89, and 0.89, respectively. On the other hand, for the RF classifier, the averaged accuracy, precision, recall, and F1 score are, respectively, 0.79, 0.78, 0.84, and 0.80. The results demonstrate that our model consistently outperforms the RF classifier across most classes in terms of accuracy, precision, recall, and F1 score. Detailed results for each class are presented below:

- Cepheids (CEP): Our model achieved an accuracy of 81.59%, significantly higher than RF's 70.56%. Precision and recall were also improved with our model at 0.84 and 0.82, compared to 0.74 and 0.71 in RF, respectively. This led to an overall better F1 score of 0.83 versus 0.72 for RF.
- RR Lyrae (RR Lyr): For RR Lyrae, our model shows an accuracy of 85.11%, compared to 75.67% for RF. Our model also performed better in terms of precision (0.87 vs. 0.77) and recall (0.85 vs. 0.76), resulting in a higher F1 score of 0.86 versus 0.76 for RF.
- Mira: Both models demonstrated high performance for Mira, but our model still had an edge with an accuracy of 98.05% compared to 94.11% for RF. Both classifiers had similar precision (0.99 vs. 0.98), but our model showed better recall (0.98 vs. 0.94). This led to a slightly higher F1 score of 0.98 for our model compared to 0.96 for RF.
- δ Scuti (dScuti): Our model performed significantly better for δ Scuti stars, with an accuracy of 80.75% compared to 58.20% for RF. While RF had slightly better precision (0.92 vs. 0.87), our model outperformed RF in recall (0.81 vs. 0.58), resulting in a higher F1 score of 0.84 compared to 0.71 for RF.
- Eclipsing Binaries: For Eclipsing Binaries, our model achieved an accuracy of 94.28%, higher than RF's 90.92%. Both precision and recall were better with our model at 0.89 and 0.94, compared to RF's 0.77 and 0.91. This led to a higher F1 score of 0.92 versus 0.84 for RF.

Figures 6 and 7 present the confusion matrices obtained from one of the runs of our model and the RF classifier, respectively. The confusion matrix of our model demonstrates that our classifier successfully recovered 88% of the true labels on average, with inter-class contamination rates below 11%. The highest confusion was observed between δ Scuti and Eclipsing variables, with 10.73% of δ Scuti stars being misclassified as Eclipsing Binaries. The misclassification is likely due to the similarities in the light curves of δ Scuti stars and Eclipsing Binaries, particularly in cases where their periods overlap. Both δ Scuti stars and EW-type Eclipsing Binaries exhibit periodic variability with relatively short periods and moderate amplitude changes. δ Scuti stars pulsate due to internal pressure-driven mechanisms, while Eclipsing Binaries experience periodic dips in brightness due to mutual eclipses of their stellar components. However, the smooth, sinusoidal-like light curve of δ Scuti stars can resemble the symmetric light curves of Eclipsing Binaries, especially Contact Binaries. This overlap in light curve features and period ranges contributes to the difficulty in distinguishing between the two types. This finding is consistent with the results reported by [37], where their classifier exhibited a 17.76% confusion rate between these classes.

Another notable misclassification occurred between Cepheids and RR Lyrae stars, where our classifier showed a misclassification rate of 10.27%. This confusion can be attributed to the similarities in the shape of their light curves, especially for short-period Cepheids, whose variability features can resemble those of RR Lyrae stars. Both types of stars exhibit asymmetric light curves with a sharp rise and a slower decline, which can lead the classifier to confuse them, particularly when their periods and amplitudes overlap. One contributing factor to this misclassification is the inclusion of all types of RR Lyrae stars in our dataset, particularly RRc (first-overtone RR Lyrae), which are often confused with first-overtone Cepheids. Both RRc stars and first-overtone Cepheids exhibit relatively short periods and similar light curve shapes, increasing the likelihood of confusion. Since the underlying pulsation mechanisms for both types are driven by the same physical processes, distinguishing between them can be challenging for automated classification systems [51]. This misclassification pattern was also observed in the findings of [37,52], where a similar

misclassification rate of 21% and 20% was reported. Remarkably, δ Scuti variables were classified by our method with $\sim$25% higher accuracy than with the RF classifier.
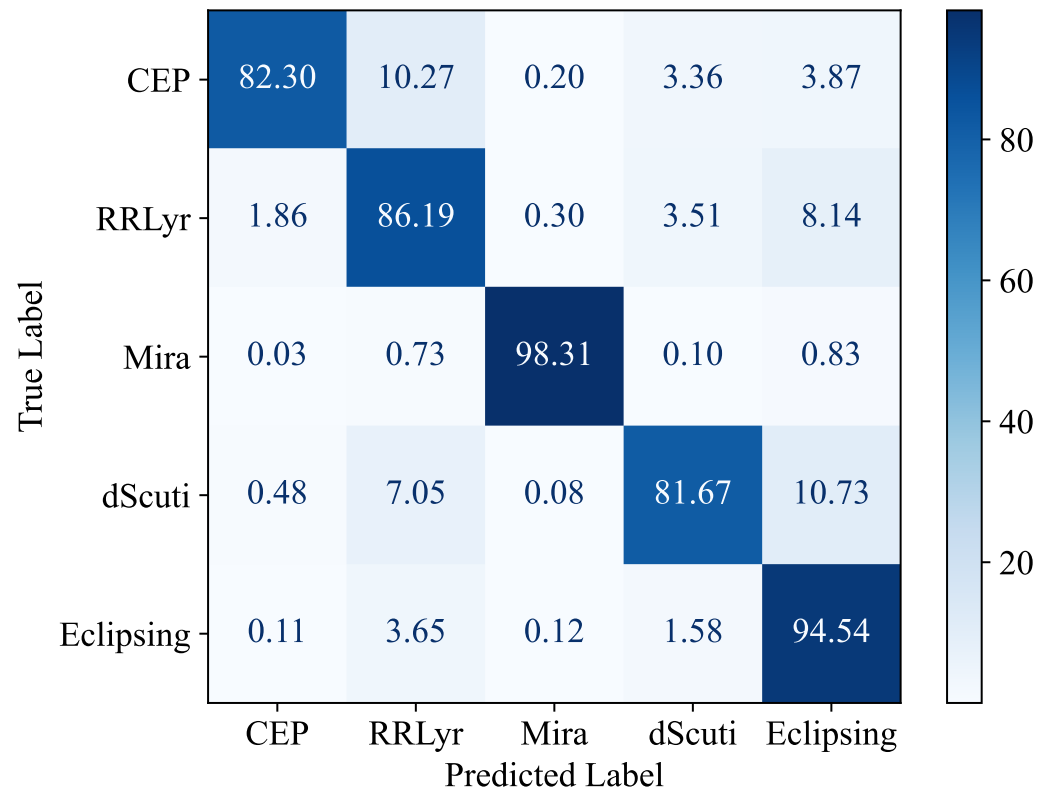

Figure 6. Classification results of our CNN model from one of the runs.
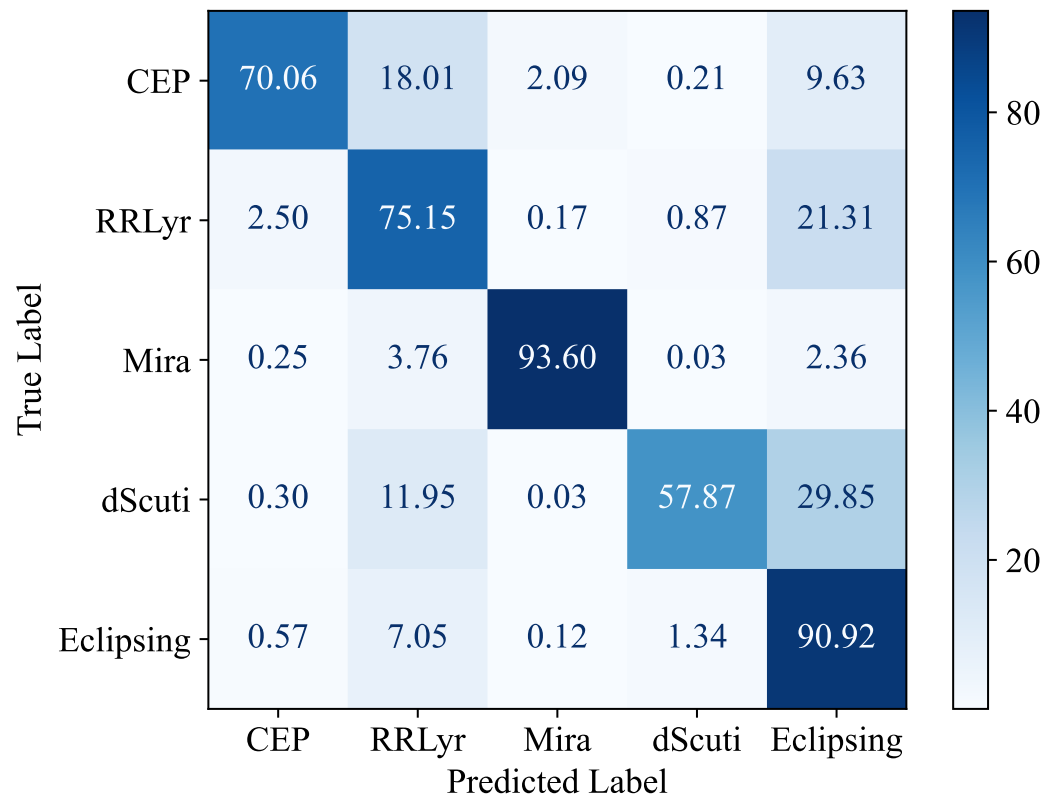

Figure 7. Classification results of RF from one of the runs.

For the case of RF, we obtained an average accuracy of 79%, implying significant confusion between classes. In particular, RF missclassified 29.9% of δ Scuti and 21.31% of RR Lyrae as Eclipsing and 18.01% of Cepheids as RR Lyrae.

The significant performance difference between our CNN model and the RF classifier can be attributed to their distinct feature extraction methodologies. CNNs automatically learn relevant features directly from raw light curves through convolutional layers, capturing complex patterns such as local variations in flux and intricate temporal behaviors. In contrast, RF relies on pre-defined features, limiting its ability to fully leverage the rich temporal information. For instance, the CNN's capacity to discern subtle differences in variability types, such as those between δ Scuti and Eclipsing Binaries, leads to better classification accuracy. In contrast, RF classifiers rely on manually engineered features like period, amplitude, and basic flux variations, which limit their ability to fully leverage the detailed temporal information contained in the light curves. This advantage reflects a more robust understanding of stellar variability processes, suggesting that the CNN model is better suited for this classification task.

As a future scope of this work, we will investigate the use of hierarchical classification methods to classify variable stars into groups and subgroups. We will also test the model on different datasets like TESS, Kepler, and WISE.

5. Conclusions

In this article, we propose a new CNN-based classifier for recognizing the type of variable stars based on light curves. This method does not require feature computation, can scale to vast amounts of data, and only needs the known periods alongside the light curves. Trained and tested on the OGLE dataset, our model demonstrates an average accuracy of 88% and an F1 score of 0.89 across five well-known classes.

In addition, we compared our classification model with a state-of-the-art RF classifier and showed that our model gives better results across all classification metrics. In particular, the improvements in accuracy, precision, recall, and F1 score are ∼9%, 0.05, 0.10, and 0.09, respectively.

Author Contributions: Conceptualization, A.A. (Almat Akhmetali) and N.U.; methodology, A.A. (Almat Akhmetali); software, T.N.; validation, N.U. and G.S.; formal analysis, G.S.; investigation, M.Z.; resources, G.S.; data curation, A.A. (Aigerim Akniyazova); writing—original draft preparation, A.A. (Almat Akhmetali); writing—review and editing, A.A. (Aigerim Akniyazova); visualization, Y.A.; supervision, N.U.; project administration, Y.A.; funding acquisition, N.U. All authors have read and agreed to the published version of the manuscript.

Institutional Review Board Statement: Not applicable.

Informed Consent Statement: Not applicable.

Data Availability Statement: The data underlying this article are available at the OGLE Collection of Variable Stars, at https://ogledb.astrouw.edu.pl/~ogle/OCVS/ (accessed on 20 August 2024).

Conflicts of Interest: The authors declare no conflicts of interest.

References

1. Feast, M. Cepheids as distance indicators. *Publ. Astron. Soc. Pac.* **1999**, *111*, 775. [CrossRef]
2. Freedman, W.L.; Madore, B.F.; Gibson, B.K.; Ferrarese, L.; Kelson, D.D.; Sakai, S.; Mould, J.R.; Kennicutt, R.C., Jr.; Ford, H.C.; Graham, J.A.; et al. Final results from the Hubble Space Telescope key project to measure the Hubble constant. *Astrophys. J.* **2001**, *553*, 47. [CrossRef]
3. Clementini, G.; Gratton, R.; Bragaglia, A.; Carretta, E.; Di Fabrizio, L.; Maio, M. Distance to the large magellanic cloud: The RR lyrae stars. *Astron. J.* **2003**, *125*, 1309. [CrossRef]
4. Vilardell, F.; Jordi, C.; Ribas, I. A comprehensive study of Cepheid variables in the Andromeda galaxy-Period distribution, blending, and distance determination. *Astron. Astrophys.* **2007**, *473*, 847–855. [CrossRef]

5. Harris, G.L.; Rejkuba, M.; Harris, W.E. The distance to NGC 5128 (Centaurus A). *Publ. Astron. Soc. Aust.* **2010**, *27*, 457–462. [CrossRef]
6. Bhardwaj, A.; Kanbur, S.M.; Macri, L.M.; Singh, H.P.; Ngeow, C.C.; Wagner-Kaiser, R.; Sarajedini, A. Large Magellanic Cloud Near-infrared Synoptic Survey. II. The Wesenheit Relations and Their Application to the Distance Scale. *Astron. J.* **2016**, *151*, 88. [CrossRef]
7. Riess, A.G.; Macri, L.M.; Hoffmann, S.L.; Scolnic, D.; Casertano, S.; Filippenko, A.V.; Tucker, B.E.; Reid, M.J.; Jones, D.O.; Silverman, J.M.; et al. A 2.4% determination of the local value of the Hubble constant. *Astrophys. J.* **2016**, *826*, 56. [CrossRef]
8. Ripepi, V.; Cioni, M.R.L.; Moretti, M.I.; Marconi, M.; Bekki, K.; Clementini, G.; de Grijs, R.; Emerson, J.; Groenewegen, M.A.; Ivanov, V.D.; et al. The VMC survey–XXV. The 3D structure of the Small Magellanic Cloud from Classical Cepheids. *Mon. Not. R. Astron. Soc.* **2017**, *472*, 808–827. [CrossRef]
9. Luck, R.; Kovtyukh, V.; Andrievsky, S. The distribution of the elements in the galactic disk. *Astron. J.* **2006**, *132*, 902. [CrossRef]
10. Pedicelli, S.; Bono, G.; Lemasle, B.; François, P.; Groenewegen, M.; Lub, J.; Pel, J.; Laney, D.; Piersimoni, A.; Romaniello, M.; et al. On the metallicity gradient of the Galactic disk. *Astron. Astrophys.* **2009**, *504*, 81–86. [CrossRef]
11. Genovali, K.; Lemasle, B.; Bono, G.; Romaniello, M.; Fabrizio, M.; Ferraro, I.; Iannicola, G.; Laney, C.; Nonino, M.; Bergemann, M.; et al. On the fine structure of the Cepheid metallicity gradient in the Galactic thin disk. *Astron. Astrophys.* **2014**, *566*, A37. [CrossRef]
12. Udalski, A.; Szymanski, M.; Kaluzny, J.; Kubiak, M.; Krzeminski, W.; Mateo, M.; Preston, G.; Paczynski, B. The optical gravitational lensing experiment. Discovery of the first candidate microlensing event in the direction of the Galactic Bulge. *Acta Astron.* **1993**, *43*, 289–294.
13. Soszynski, I.; Udalski, A.; Szymanski, M.; Skowron, D.; Pietrzynski, G.; Poleski, R.; Pietrukowicz, P.; Skowron, J.; Mróz, P.; Kozłowski, S.; et al. The OGLE Collection of Variable Stars. Classical Cepheids in the Magellanic System. *Acta Astron.* **2015**, *65*, 297–312.
14. Soszyński, I.; Udalski, A.; Szymański, M.; Wyrzykowski, Ł.; Ulaczyk, K.; Poleski, R.; Pietrukowicz, P.; Kozłowski, S.; Skowron, D.; Skowron, J.; et al. The OGLE Collection of Variable Stars. Over 45 000 RR Lyrae Stars in the Magellanic System. *Acta Astron.* **2016**, *66*, 131–147.
15. Ulaczyk, K.; Poleski, R.; Pietrukowicz, P.; Kozłowski, S.; Skowron, D.; Skowron, J.; Mróz, P.; Rybicki, K. The OGLE collection of variable stars. Type II cepheids in the magellanic system. *Acta Astron.* **2018**, *68*, 89–109.
16. Pojmanski, G.; Pilecki, B.; Szczygieł, D. The All Sky Automated Survey. Catalog of Variable Stars. V. Declinations 0°–+28° of the Northern Hemisphere.
    Acta Astron. **2005**, *55*, 275–301.
17. Drake, A.; Djorgovski, S.; Mahabal, A.; Beshore, E.; Larson, S.; Graham, M.; Williams, R.; Christensen, E.; Catelan, M.; Boattini, A.; et al. First results from the catalina real-time transient survey. *Astrophys. J.* **2009**, *696*, 870. [CrossRef]
18. Djorgovski, S.G.; Donalek, C.; Mahabal, A.; Moghaddam, B.; Turmon, M.; Graham, M.; Drake, A.; Sharma, N.; Chen, Y. Towards an automated classification of transient events in synoptic sky surveys. *arXiv* **2011**, arXiv:1110.4655.
19. Graham, M.J.; Kulkarni, S.R.; Bellm, E.C.; Adams, S.M.; Barbarino, C.; Blagorodnova, N.; Bodewits, D.; Bolin, B.; Brady, P.R.; Cenko, S.B.; et al. The Zwicky transient facility: Science Objectives. *Publ. Astron. Soc. Pac.* **2019**, *131*, 078001. [CrossRef]
20. Bellm, E.C.; Kulkarni, S.R.; Graham, M.J.; Dekany, R.; Smith, R.M.; Riddle, R.; Masci, F.J.; Helou, G.; Prince, T.A.; Adams, S.M.; et al. The Zwicky Transient Facility: System overview, performance, and first results. *Publ. Astron. Soc. Pac.* **2018**, *131*, 018002. [CrossRef]
21. Basri, G.; Borucki, W.J.; Koch, D. The Kepler Mission: A wide-field transit search for terrestrial planets. *New Astron. Rev.* **2005**, *49*, 478–485. [CrossRef]
22. Ferreira Lopes, C.; Cross, N. New insights into time series analysis. II-Non-correlated observations. *Astron. Astrophys.* **2017**, *604*, A121. [CrossRef]
23. Debosscher, J.; Sarro, L.; Aerts, C.; Cuypers, J.; Vandenbussche, B.; Garrido, R.; Solano, E. Automated supervised classification of variable stars-I. methodology. *Astron. Astrophys.* **2007**, *475*, 1159–1183. [CrossRef]
24. Kim, D.W.; Protopapas, P.; Byun, Y.I.; Alcock, C.; Khardon, R.; Trichas, M. Quasi-stellar object selection algorithm using time variability and machine learning: Selection of 1620 quasi-stellar object candidates from MACHO Large Magellanic Cloud database. *Astrophys. J.* **2011**, *735*, 68. [CrossRef]
25. Alcock, C.; Allsman, R.; Axelrod, T.; Bennett, D.; Cook, K.; Freeman, K.; Griest, K.; Guern, J.; Lehner, M.; Marshall, S. The MACHO project first year LMC results: The Microlensing rate and the nature of the galactic dark halo. *Astrophys. J.* **1996**, *461*, 84. [CrossRef]
26. Breiman, L. Random forests. *Mach. Learn.* **2001**, *45*, 5–32. [CrossRef]
27. Cortes, C. Support-Vector Networks. *Mach. Learn.* **1995**, *20*, 273–297. [CrossRef]
28. Richards, J.W.; Starr, D.L.; Butler, N.R.; Bloom, J.S.; Brewer, J.M.; Crellin-Quick, A.; Higgins, J.; Kennedy, R.; Rischard, M. On machine-learned classification of variable stars with sparse and noisy time-series data. *Astrophys. J.* **2011**, *733*, 10. [CrossRef]
29. Butler, N.R.; Bloom, J.S. Optimal time-series selection of quasars. *Astron. J.* **2011**, *141*, 93. [CrossRef]
30. Kim, D.W.; Bailer-Jones, C.A. A package for the automated classification of periodic variable stars. *Astron. Astrophys.* **2016**, *587*, A18. [CrossRef]
31. Elorrieta, F.; Eyheramendy, S.; Jordán, A.; Dékány, I.; Catelan, M.; Angeloni, R.; Alonso-García, J.; Contreras-Ramos, R.; Gran, F.; Hajdu, G.; et al. A machine learned classifier for RR Lyrae in the VVV survey. *Astron. Astrophys.* **2016**, *595*, A82. [CrossRef]

32. Gran, F.; Minniti, D.; Saito, R.; Zoccali, M.; Gonzalez, O.; Navarrete, C.; Catelan, M.; Ramos, R.C.; Elorrieta, F.; Eyheramendy, S.; et al. Mapping the outer bulge with RRab stars from the VVV Survey. *Astron. Astrophys.* **2016**, *591*, A145. [CrossRef]
33. Mahabal, A.; Sheth, K.; Gieseke, F.; Pai, A.; Djorgovski, S.G.; Drake, A.J.; Graham, M.J. Deep-learnt classification of light curves. In Proceedings of the 2017 IEEE Symposium Series on Computational Intelligence (SSCI), Honolulu, HI, USA, 27 November–1 December 2017; IEEE: Piscataway, NJ, USA, 2017; pp. 1–8.
34. Naul, B.; Bloom, J.S.; Pérez, F.; Van Der Walt, S. A recurrent neural network for classification of unevenly sampled variable stars. *Nat. Astron.* **2018**, *2*, 151–155. [CrossRef]
35. Aguirre, C.; Pichara, K.; Becker, I. Deep multi-survey classification of variable stars. *Mon. Not. R. Astron. Soc.* **2019**, *482*, 5078–5092. [CrossRef]
36. Carrasco-Davis, R.; Cabrera-Vives, G.; Förster, F.; Estévez, P.A.; Huijse, P.; Protopapas, P.; Reyes, I.; Martínez-Palomera, J.; Donoso, C. Deep learning for image sequence classification of astronomical events. *Publ. Astron. Soc. Pac.* **2019**, *131*, 108006. [CrossRef]
37. Becker, I.; Pichara, K.; Catelan, M.; Protopapas, P.; Aguirre, C.; Nikzat, F. Scalable end-to-end recurrent neural network for variable star classification. *Mon. Not. R. Astron. Soc.* **2020**, *493*, 2981–2995. [CrossRef]
38. Zorich, L.; Pichara, K.; Protopapas, P. Streaming classification of variable stars. *Mon. Not. R. Astron. Soc.* **2020**, *492*, 2897–2909. [CrossRef]
39. Hinton, G.E.; Salakhutdinov, R.R. Reducing the dimensionality of data with neural networks. *Science* **2006**, *313*, 504–507. [CrossRef]
40. Bengio, Y. Learning Deep Architectures for AI. *Found. Trends Mach. Learn.* **2009**, *2*, 1–127. [CrossRef]
41. LeCun, Y.; Bengio, Y.; Hinton, G. Deep learning. *Nature* **2015**, *521*, 436–444. [CrossRef]
42. Dieleman, S.; Willett, K.W.; Dambre, J. Rotation-invariant convolutional neural networks for galaxy morphology prediction. *Mon. Not. R. Astron. Soc.* **2015**, *450*, 1441–1459. [CrossRef]
43. Fabbro, S.; Venn, K.; O'Briain, T.; Bialek, S.; Kielty, C.; Jahandar, F.; Monty, S. An application of deep learning in the analysis of stellar spectra. *Mon. Not. R. Astron. Soc.* **2018**, *475*, 2978–2993. [CrossRef]
44. Metcalf, R.B.; Meneghetti, M.; Avestruz, C.; Bellagamba, F.; Bom, C.R.; Bertin, E.; Cabanac, R.; Courbin, F.; Davies, A.; Decencière, E.; et al. The strong gravitational lens finding challenge. *Astron. Astrophys.* **2019**, *625*, A119. [CrossRef]
45. Kim, E.J.; Brunner, R.J. Star-galaxy classification using deep convolutional neural networks. *Mon. Not. R. Astron. Soc.* **2016**, *464*, 4463–4475. [CrossRef]
46. Sharma, K.; Kembhavi, A.; Kembhavi, A.; Sivarani, T.; Abraham, S.; Vaghmare, K. Application of convolutional neural networks for stellar spectral classification. *Mon. Not. R. Astron. Soc.* **2020**, *491*, 2280–2300. [CrossRef]
47. Ussipov, N.; Zhanabaev, Z.; Akhmetali, A.; Zaidyn, M.; Turlykozhayeva, D.; Akniyazova, A.; Namazbayev, T. Classification of Gravitational Waves from Black Hole-Neutron Star Mergers with Machine Learning. *J. Astron. Space Sci.* **2024**, *41*, 149–158. [CrossRef]
48. Abadi, M.; Agarwal, A.; Barham, P.; Brevdo, E.; Chen, Z.; Citro, C.; Corrado, G.S.; Davis, A.; Dean, J.; Devin, M.; et al. Tensorflow: Large-scale machine learning on heterogeneous distributed systems. *arXiv* **2016**, arXiv:1603.04467.
49. Kingma, D.P. Adam: A method for stochastic optimization. *arXiv* **2014**, arXiv:1412.6980.
50. Pedregosa, F.; Varoquaux, G.; Gramfort, A.; Michel, V.; Thirion, B.; Grisel, O.; Blondel, M.; Prettenhofer, P.; Weiss, R.; Dubourg, V.; et al. Scikit-learn: Machine learning in Python. *J. Mach. Learn. Res.* **2011**, *12*, 2825–2830.
51. Chen, X.; Wang, S.; Deng, L.; De Grijs, R.; Yang, M.; Tian, H. The Zwicky transient facility catalog of periodic variable stars. *Astrophys. J. Suppl. Ser.* **2020**, *249*, 18. [CrossRef]
52. Bassi, S.; Sharma, K.; Gomekar, A. Classification of variable stars light curves using long short term memory network. *Front. Astron. Space Sci.* **2021**, *8*, 718139. [CrossRef]